Cancer Letters 499 (2021) 220–231

Contents lists available at ScienceDirect

Cancer Letters

journal homepage: www.elsevier.com/locate/canlet

Glabrescione B delivery by self-assembling micelles efficiently inhibits tumor growth in preclinical models of Hedgehog-dependent medulloblastoma

Paola Infante [a,1], Alessio Malfanti [b,1], Deborah Quaglio [c,1], Silvia Balducci [c], Sara De Martin [b], Francesca Bufalieri [d], Francesca Mastrotto [b], Irene Basili [d], Mariangela Garofalo [b], Ludovica Lospinoso Severini [d], Mattia Mori [e], Isabella Manni [f], Marta Moretti [g], Carmine Nicoletti [h,i], Giulia Piaggio [f], Paolo Caliceti [b], Bruno Botta [c], Francesca Ghirga [a,***], Stefano Salmaso [b,**], Lucia Di Marcotullio [d,i,*]

[a] Center for Life Nano Science@Sapienza, Istituto Italiano di Tecnologia, Roma, Italy
[b] Department of Pharmaceutical and Pharmacological Sciences, University of Padova, Padova, Italy
[c] Department of Chemistry and Technology of Drugs, University La Sapienza, Roma, Italy
[d] Department of Molecular Medicine, University La Sapienza, Roma, Italy
[e] Department of Biotechnology, Chemistry and Pharmacy, University of Siena, Siena, Italy
[f] UOSD SAFU, Department of Research, Diagnosis and Innovative Technologies, IRCCS-Regina Elena National Cancer Institute, Roma, Italy
[g] Department of Experimental Medicine, University La Sapienza, Roma, Italy
[h] DAHFMO-Unit of Histology and Medical Embryology, University La Sapienza, Roma, Italy
[i] Laboratory Affiliated to Istituto Pasteur Italia-Fondazione Cenci Bolognetti, Department of Molecular Medicine, University La Sapienza, Roma, Italy

ARTICLE INFO

Keywords:
Hedgehog signaling pathway
GLI inhibitor
Drug delivery
Pharmacology
Medulloblastoma

ABSTRACT

Aberrant activation of the Hedgehog (Hh) pathway leads to the development of several tumors, including medulloblastoma (MB), the most common pediatric brain malignancy. Hh inhibitors acting on GLI1, the final effector of Hh signaling, offer a valuable opportunity to overcome the pitfalls of the existing therapies to treat Hh-driven cancers. In this study, the toxicity, delivery, biodistribution, and anticancer efficacy of Glabrescione B (GlaB), a selective GLI1 inhibitor, were investigated in preclinical models of Hh-dependent MB. To overcome its poor water solubility, GlaB was formulated with a self-assembling amphiphilic polymer forming micelles, called $mPEG_{5kDa}$-cholane. $mPEG_{5kDa}$-cholane/GlaB showed high drug loading and stability, low cytotoxicity, and long permanence in the bloodstream. We found that $mPEG_{5kDa}$-cholane efficiently enhanced the solubility of GlaB, thus avoiding the use of organic solvents. $mPEG_{5kDa}$-cholane/GlaB possesses favorable pharmacokinetics and negligible toxicity. Remarkably, GlaB encapsulated in $mPEG_{5kDa}$-cholane micelles was delivered through the blood-brain barrier and drastically inhibited tumor growth in both allograft and orthotopic models of Hh-dependent MB. Our findings reveal that $mPEG_{5kDa}$-cholane/GlaB is a good candidate for the treatment of Hh-driven tumors and provide relevant implications for the translation of GlaB into clinical practice.

1. Introduction

Hedgehog (Hh) signaling is a developmental pathway whose deregulation is responsible for several malignancies and is emerging as a druggable pathway for the treatment of a wide spectrum of cancers [1].

Medulloblastoma (MB) is one of the most common Hh-dependent tumors. It is a highly aggressive pediatric brain malignancy that arises in the cerebellum and is caused by genetic mutations or chromosomal

Abbreviations: (Hh), Hedgehog; (MB), Medulloblastoma; (GLI1), Glioma-associated oncogene 1; (GlaB), Glabrescione B; (HPLC), High-Performance Liquid Chromatography; (BBB), blood-brain barrier; (PK), pharmacokinetic; (HP-βCD), hydroxypropyl β-cyclodextrin.

* Corresponding author. Department of Molecular Medicine, University La Sapienza, Roma, Italy.
** Corresponding author.
*** Corresponding author.
E-mail addresses: francesca.ghirga@iit.it (F. Ghirga), stefano.salmaso@unipd.it (S. Salmaso), lucia.dimarcotullio@uniroma1.it (L. Di Marcotullio).

[1] P. Infante, A. Malfanti and D. Quaglio contributed equally to this article.

https://doi.org/10.1016/j.canlet.2020.11.028
Received 21 August 2020; Received in revised form 20 November 2020; Accepted 23 November 2020
Available online 26 November 2020

alterations involving key components of Hh signaling [2].

According to the current molecular classification, MB is divided into four main subgroups: Wnt, Hh, Group 3, and Group 4. The Hh subgroup (Hh-MB) accounts for 30% of MB cases and is one of the most significant potential targets for the clinical exploitation of Hh pathway inhibitors [3,4].

The canonical activation of Hh signaling is triggered by the interaction of an Hh ligand with the Pathched1 (PTCH1) receptor, which relieves the inhibition of the co-receptor Smoothened (SMO), leading to the activation of the downstream GLI transcription factors (GLI1, GLI2, and GLI3) [5]. GLI proteins regulate important cellular processes that trigger the expression of several target genes, including *GLI1,* generating an autoregulatory loop that enhances the Hh response [6]. Although many Hh-dependent cancers involve upstream pathway activation (i.e., loss-of-function *PTCH1* or *SUFU* or gain-of-function *SMO* mutations), many others occur via a non-canonical Hh pathway activation, which is SMO-independent and related to increased function of the downstream GLI effectors (i.e., *GLI1* gene amplification, chromosomal translocation, or GLI2 protein stabilization) [7–9].

For this reason, the main therapeutic strategies for the treatment of Hh-dependent tumors have been based on the inhibition of SMO and GLIs, in order to block the Hh pathway both at upstream and downstream levels, respectively [10]. At present, three SMO antagonists have been approved by the Food and Drug Administration (FDA) as therapy for metastatic or locally advanced basal cell carcinoma (Vismodegib and Sonidegib) and acute myeloid leukemia (Glasdegib) [11]. Despite good initial efficacy, they have shown several side effects and limitations, including the onset of *SMO* drug-resistant mutations with consequent relapse of tumor [12]. These pitfalls necessitate the development of new Hh inhibitors that can block pathway signaling downstream by acting on the transcription factor GLI1, the final and most powerful effector of Hh signaling. GLI1 controls the expression of genes whose deregulation is responsible for cell transformation and tumor progression, such as *CCND1*, *CCND2*, *MYCN*, *PDGFR*, *IGF2,* and *BCL2,* which promote proliferation and cell survival, *VEGF* and *SNAIL,* which regulate angiogenesis and epithelial-to-mesenchymal transition (EMT), respectively, and *NANOG* and *BMI*, which control self-renewal and cell fate [13].

However, only a few GLI inhibitors have been identified to date [10]. Our research group has recently discovered unique bio-activities of Glabrescione B (GlaB), a natural compound found in *Derris glabrescens* (*Leguminosae*) seeds, as the first small molecule to bind directly to GLI1 and to inhibit its interaction with DNA. We showed that GlaB reduces tumor growth both *in vitro* and *in vivo* in MB and BCC models depending on specific Hh-activating mutation (*Ptch1* loss-of-function) and is thus a good candidate for pre-clinical investigations in the treatment of Hh-driven cancers [14].

Here, we demonstrated that GlaB does not possess toxic and unspecificied effects on the proliferation of non-target tissues in a transgenic reporter mouse model, MITO-Luc [15]. Furthermore, we developed a colloidal formulation of GlaB to ameliorate its biopharmaceutical properties due to its poor solubility. Additionally, we assessed whether that the encapsulation of GlaB in mPEG$_{5kDa}$-cholane based micelles increased its solubility, biodistribution, and effectiveness in inhibiting Hh-dependent MB growth in mouse models. Moreover, High-Performance Liquid Cromatography (HPLC) analysis revealed that the drug loaded in mPEG$_{5kDa}$-cholane based micelles upon intravenous administration crosses the blood-brain barrier (BBB), thus reducing *in situ* MB growth.

Overall, these findings indicate mPEG$_{5kDa}$-cholane/GlaB formulation as an interesting candidate for clinical studies for the treatment of Hh-dependent cancers, such as Hh-MB.

2. Materials and methods

2.1. Reagents

5-β-cholanic acid, cholesterol, cholesterol hemisuccinate, *N*–N′-dimethylformamide (DMF), chloroform, toluene, trimethylamine (TEA) and deuterated solvent ($CDCl_3$), formic acid (FA) were purchased from Sigma-Aldrich (St. Louis, MO, USA). Dichloromethane (DCM), methanol (MeOH), acetonitrile (ACN) and diethyl ether were obtained from Scharlab S.L. (Gato Peres, Barcellona, Spain). Linear 5 kDa α-methoxy-ω-amino-polyethylene glycol (mPEG$_{5kDa}$-NH$_2$) was purchased from Iris Biotech GmbH (Marktredwitz, Germany). α-Methoxy-5kDa polyethylene glycol-ω-distearoyl phosphatidylethanolamine (mPEG$_{5kDa}$-DSPE) was obtained from Laysan Bio (Arab, Alabama, USA). Salts and buffers were purchased from Fluka Analytical (Buchs SG, Switzerland) and Sigma-Aldrich. Tween® 80 and Tween® 20 were purchased from Fluka Analytical. Hydroxypropyl β-cyclodextrin (HP-βCD) was acquired from Roquette (Lestrem, France). Cremophor® EL, Pluronic F-127 and PEG$_{400}$ were purchased from Sigma-Aldrich.

RPMI-1640, glutamine solution, penicillin-streptomycin solution, sodium pyruvate, non-essential amino acids, bovin serum albumin (BSA) and lipopolysaccharides (LPS), obtained from *Escherichia Coli* serotype O26:B6 were purchased from Sigma-Aldrich.

All the other reagents or salts were obtained from Fluka Analytical or Sigma-Aldrich.

2.2. Synthesis of mPEG$_{5kDa}$-cholane, mPEG$_{5kDa}$-cholesterol, and Glabrescione B

mPEG$_{5kDa}$-cholane was obtained and characterized according to the procedure reported elsewhere [16,17]. The synthesis and characterization of methoxy(polyethylene glycol$_{5kDa}$)-cholesteryl-hemisuccinate (mPEG$_{5kDa}$-cholesterol) were performed as reported in the literature [18].

Glabrescione B was prepared according to the synthetic procedure reported previously [19]. The structure was unambiguously confirmed through nuclear magnetic resonance (NMR) spectroscopy and by electrospray ionization-high- resolution mass spectrometry (ESI-HRMS).

2.3. Glabrescione B solubility studies

GlaB solubility in water in the presence of increasing concentration of amphiphilic polymers was evaluated by thin-film hydration procedure according to the protocol described by Bangham et al. [20]. Briefly, 250 μL of 2.0 mg/mL (4.4 μM) GlaB solution in methanol was mixed with 100 μL of 0.1–5 mM mPEG$_{5kDa}$-cholane or mPEG$_{5kDa}$-cholesterol solutions in methanol. The organic solvent was removed under vacuum and the resulting polymeric films were hydrated with 250 μL of 10 mM phosphate, 0.15 M NaCl, pH 7.4. The samples were mixed using a rotatory mixer for 48 h and then centrifuged for 10 min at 14,000 rpm. GlaB concentration in the supernatants was assessed by RP-HPLC using a Jasco system (Easton, MD, USA) equipped with a Phenomenex Luna C18 reverse-phase column (5 μm, 100 Å, 250 × 4.6 mm). The column was eluted with MilliQ water (eluent A) and acetonitrile (eluent B) both added of 0.05% v/v trifluoroacetic acid in a gradient mode from 50% to 95% eluent B in 21 min at a flow rate of 1 mL/min. The UV–Vis detector UV-2075 Plus (Jasco system, Easton, MD, USA) was set at 295 nm and GlaB was eluted at 17 min. The GlaB concentration was derived from a calibration line ($y = 38893x - 533.07$, $R^2 = 0.9995$) previously generated using standard solutions at increasing concentration of GlaB in acetonitrile. The areas of eluted GlaB peaks were integrated using Borwin Chromatography 1.5 software (Jasco system; Easton, MD, USA). The GlaB dissolution in the presence of mPEG$_{5kDa}$-NH$_2$, Tween® 80, mPEG$_{5kDa}$-DSPE and Pluronic F-127 was assessed by using the procedure reported above. The GlaB solubility in the presence of hydroxypropyl β-cyclodextrin (HP-βCD) was determined by adding 250 μL of 0.04–2

mM HP-βCD solutions in 10 mM phosphate, 0.15 M NaCl, pH 7.4 to vials containing 0.5 mg of solid GlaB. The mixtures were stirred for 48 h and then centrifuged for 10 min at 14,000 rpm, and GlaB concentration in the supernatants was assessed as reported above.

2.4. Formulation of $mPEG_{5kDa}$-cholane and $mPEG_{5kDa}$-cholesterol based micelles

A 1 mL volume of a GlaB solution (2.0 mg/mL, 4.4 mM) in methanol was added to 1 mL of $mPEG_{5kDa}$-cholane or $mPEG_{5kDa}$-cholesterol solution (6.0 mg/mL, 1.2 mM) in methanol. The organic solvent was removed under reduced pressure and 1 mL of 10 mM phosphate, 0.15 M NaCl, pH 7.4 was added to hydrate the polymeric film. The mixture was left in a rotary mixer for 48 h and then centrifuged for 10 min at 14,000 rpm to remove the undissolved GlaB. The supernatant was collected and analyzed to assess GlaB concentration by RP-HPLC as described above.

2.5. GlaB release study

1 mL samples of GlaB-loaded $mPEG_{5kDa}$-cholane and $mPEG_{5kDa}$-cholesterol micelles (0.71 mM GlaB, 3.5 mg/mL of $mPEG_{5kDa}$-cholane and 6 mg/mL of $mPEG_{5kDa}$-cholesterol micelles, respectively) in 10 mM phosphate, 150 mM NaCl, pH 7.4 were transferred into a 3.5–5 kDa MWCO Float-A-Lyzer and dialyzed against 5 L of 10 mM phosphate, 150 mM NaCl, pH 7.4, supplemented of 0.5% w/v of Pluronic F-127. The external medium was replaced three times a day with fresh buffer. At scheduled time points, 20 μL volumes were withdrawn from the dialysis bag and the GlaB concentration was assessed by RP-HPLC as reported above.

2.6. Biocompatibility of $mPEG_{5kDa}$-cholane or $mPEG_{5kDa}$-cholesterol

Effect of GlaB-loaded micelles on proteins. The effect of $mPEG_{5kDa}$-cholane and $mPEG_{5kDa}$ cholesterol micelles on the conformational structure of bovine serum albumin (BSA) was evaluated according to the procedure reported by Luengo-Alonso et al. [21]. Briefly, 2 μM of BSA solutions in 10 mM phosphate, 150 mM NaF, pH 7.4 in the presence of GlaB-loaded $mPEG_{5kDa}$-cholane and $mPEG_{5kDa}$-cholesterol micelles (0.5 mg/mL) were incubated for 1 h at room temperature and analyzed at 25 °C by circular dichroism (CD) in the far UV (from 198 to 300 nm, 50 nm/s with 8 s response and 2 nm bandwidth) using a J-810 Jasco spectrodichrograph (Jasco, Tokyo, Japan). The data were processed using CD Spectra Deconvolution software.

Hemolysis assay. Mouse blood (2 mL) was added of 100 μL of 5000 U. I./mL heparin solution (Teva pharmaceutical LTD, Petach Tikva, Israel) and centrifuged at 800 g for 5 min at 4 °C. Plasma was discarded and the red blood cell (RBCs) pellet was re-dispersed in 10 mL of 10 mM phosphate, 150 mM NaCl, pH 7.4, and washed three times with the same buffer. A 2% w/w final RBCs suspension was prepared and incubated with increasing concentrations of $mPEG_{5kDa}$-cholane or $mPEG_{5kDa}$-cholesterol (0.01–1 mg/mL) at 37 °C for 1 h [22]. Ten kDa Dextran in the same range of concentration was used as non-hemolytic control while 1 v/v% Triton X-100 in the same buffer was used as positive control. The samples were centrifuged at 1100 rpm for 5 min and 100 μL of the supernatants was transferred into a 96-well plate. The absorbance was measured at 570 nm using Microplate Autoreader EL311 (Bio--Tek-Instruments, Winooski, VT, USA).

The percentage of hemolysis was normalized to that of RBCs incubated with the Triton X-100 solution (100% hemolysis).

2.7. Cytotoxicity and cell proliferation assays

Daoy cells (human medulloblastoma cell line from ATCC, Manassas, VA, USA) were cultured at 37 °C in Minimum Essential Medium Eagle (MEM) medium supplemented with 2 mM L-glutamine, 1 mM sodium pyruvate, 100 IU/mL penicillin, 100 μg/mL streptomycin, and 0.25 μg/mL of amphotericin B, 10% (v/v) heat-inactivated fetal bovine serum (FBS), with a 5% CO_2 atmosphere. The cells were harvested by treatment with 0.05% (w/v) trypsin 0.02% (w/v) EDTA solution (Sigma-Aldrich), suspended in culture medium and seeded at the appropriate cell concentration.

In a 96-well tissue culture plate, 3×10^3 cells/well were seeded in complete MEM medium and after 24 h the medium was removed, cells washed 3 times with PBS and 200 μL of complete medium containing either $mPEG_{5kDa}$-cholane or $mPEG_{5kDa}$-cholesterol in the range 1–8.4 μM was added to each well. Cells were incubated for 12, 24, 48, and 72 h and then the medium was discarded, and cells washed 3 times with PBS. A 200 μL volume of complete medium was added per well followed by 20 μL of a 5 mg/mL 3-(4,5-dimethylthiazol-2-yl)-2,5-diphenyltetrazolium bromide (MTT) solution in PBS and cells were incubated at 37 °C for 3 h. Afterwards, the MTT-containing medium was removed, and 200 μL of DMSO was added to each well to dissolve the formazan crystals formed by the live cells. The plates were gently shaken for 30 min, and the absorbance was measured at 570 nm using an EL311SK Microplate Autoreader (Biotek Instruments Inc., VT, USA). The cell viability was derived with respect to the viability of untreated cells, which was used as a reference.

The growth rate of viable murine primary MB cells isolated from Math1-cre/$Ptc^{C/C}$ mice (The Jackson Laboratory, Bar Harbor, ME, USA/EMMA, Monterotondo, Italy) was tested by trypan blue count after incubation for 24, 48, and 72 h with the $mPEG_{5kDa}$-cholane/GlaB or $mPEG_{5kDa}$-cholesterol/GlaB formulations in the 0.5–5 μM concentration range. Tumors from Math1-cre/$Ptc^{C/C}$ mice were collected as previously described [14] and freshly prepared MB cell suspensions were used for short-term cultures to keep Hh-sensitivity *in vitro* [23]. Primary MB cells were cultured in Neurobasal-A medium with B27 supplement minus Vitamin A. Mycoplasma contamination was routinely detected by using PCR detection kit (Applied Biological Materials, Richmond, BC, Canada).

2.8. GLI-dependent luciferase reporter assay

Inhibition of GLI1-induced transcription was assessed in wild type MEFs transfected with 12xGliBS-Luc and pRL-TK Renilla (as normalization control) plus control (empty) or GLI1 vector and treated for 24 h with increasing concentrations of $mPEG_{5kDa}$-cholane/GlaB formulations. Luciferase and Renilla activities were assayed with a dual-luciferase assay system according to the manufacturer's instructions (Biotium Inc., Hayward, CA, USA). Results were expressed as luciferase/Renilla ratios and represented the mean ± S.D. of three experiments, each performed in triplicate.

2.9. Pharmacokinetic study

All the procedures involving animals were conducted in agreement with national and international regulations (D.lgs 26/2014, Directive 2010/63/EU), and suitable procedures were taken to minimize animal pain or discomfort. The procedures were reviewed and approved by the Ethical Committee of the University of Padova (OPBA), and by the Italian Ministry of Health, section for the care and use of laboratory animals (Authorization No. 858/2017, obtained on November 3, 2017). C57BL/6J mice (10±1week old) were housed in a temperature and humidity-controlled room under a constant 12 h light/dark cycle, with free access to water and food. The animals were randomly assigned to two experimental groups (n = 4) and 2.5 mg/kg of 0.31 mg/mL GlaB in 3.3% v/v of DMSO, 3% v/v of Cremophor, 4% v/v of Tween® 80, 15% v/v of PEG_{400}, 20 mM phosphate buffer, 0.15 M NaCl, pH 7.4, or GlaB equivalent dose of $mPEG_{5kDa}$-cholane/GlaB micelles in 20 mM phosphate buffer, 0.15 M NaCl, pH 7.4, were intravenously injected into the caudal vein. Blood samples (0.1 mL) were collected from the submandibular plexus at regular intervals using heparinized tubes: 0.083, 0.5, 1, 2, 4, 6, and 24 h after administration. During blood sampling, mice were

kept under anesthesia with isoflurane. The blood samples were centrifuged for 3 min at 2000 rpm and GlaB in plasma was assessed using a 3000 UltiMate HPLC (Thermo Fisher Scientific, Whaltam, MA, USA) coupled to an AP 4000 Applied Biosystems LC-MS system (Sciex, Framingham, MA, US). Ten μL of plasma were added to 290 μL of acetonitrile supplemented with 0.5 μg/mL of benzanilide (internal standard) and centrifuged at 3700 rpm for 15 min. The supernatant was analyzed by using a reversed-phase column Phenomenex Gemini C18 (5 μm, 110 Å 50 × 2 mm) eluted with ammonium formate buffer (10 mM, pH 3.5, eluent A) and acetonitrile (eluent B) with the following gradient: from 60% to 95% of eluent B in 1 min. The flow was 0.3 mL/min. The GlaB concentration was derived from a calibration curve ($y = 0.00188x + 0.00281$, $R^2 = 0.9993$) obtained using 60-36,000 pg/mL GlaB solutions in plasma. GlaB plasma concentration *vs* time data were analyzed using GraphPad Prism 8.0 software (San Diego, CA, USA) according to the Akaike Information Criterion. A bi-exponential equation was the best-fitting model for all the pharmacokinetic data obtained in this study. Pharmacokinetic parameters were calculated from the coefficients and exponents of the best-fits by using standard formulae [24].

2.10. Biodistribution of GlaB in the brain and the cerebellum

Sample preparation. HPLC analyses were performed on brain and cerebellum samples from CD1 WT mice (Charles River Laboratories, Lecco, Italy) treated with $mPEG_{5kDa}$-cholane/GlaB (9 mg/kg) by i.v. injection. After the indicated treatment times (30 min, 1, 2 and 4 h), animals were sacrificed, and the brain and the cerebellum were explanted, and organ samples were stored at −80 °C for 24 h. The day after, the brain and cerebellum samples (500 mg of tissue) were homogenized in 1 mL of PBS, using an ultrasound probe (Bandelin Sonopuls MS70, Germany). A solution of $ZnSO_4$ (0,1 M in H_2O, 1 mL) and acetonitrile (1 mL) were added to the mixture that was further homogenized with ultrasound for 15 min. Subsequently, the brain and cerebellum homogenates were stirred for 1 h at room temperature, centrifuged at 3000×*g* for 5 min at 4 °C, and the supernatants were collected. The following procedure to obtain a brain/cerebellum extract was repeated twice. Acetonitrile (1 mL) was added to the brain/cerebellum pellet, stirred for 30 min at room temperature, then centrifuged at 3000×*g* for 5 min at 4 °C and the supernatant collected. Brain and cerebellum extracts samples were centrifuged for 5 min at 5000×*g* and 20 μL of supernatant injected into the HPLC-MS without further treatments.

HPLC-MS Analysis. Analyses were performed on an Ultimate 3000 ultra-high performance liquid chromatography (HPLC) system (Thermo Fisher, Milan, Italy). The Ultimate 3000 HPLC was operated using a WPS-3000 TRS autosampler, LPG-3400RS low pressure mixing biocompatibile gradient pump with integrated analytical four channel vacuum degasser and a photo diode array detector DAD 3000RS DETECTOR (equipped with an analytical flow cell of 13 μL). The system was controlled by Chromeleon 7.2 software (Thermo Fisher, Milan, Italy). The HPLC system was equipped with a Titan™ C18 column (Supelco, Bellefonte, PA, USA), packed with 1.9 μm fully porous particles (FPP) of narrow particle size distribution, with high surface area of 400 m^2/g and average pore size of 80 Å, and a core-shell column Ascentis Express™ 100 mm × 3.0 mm 2.0 μm (Supelco, Bellefonte, PA, USA). All chromatographic runs were performed at a flow-rate of 0.4 mL/min with the column equilibrated at 35 °C. Solvent A was Water/Acetonitrile 90:10 with 0.1% v/v of formic acid, and solvent B was Acetonitrile/Methanol 50:50 with 0.1% v/v of formic acid. The chromatographic runs were performed using a gradient mode with solvent B increasing from 20 to 50% in 1 min, then 50% of solvent B was run for 3 min, finally solvent B was increased to 100% in 30 min. The LC was directly interfaced to electrospray ionization (ESI) source coupled with a Single Quadrupole-MSQ Plus Detector. Ion source was operated in positive ESI mode and both Full Scan and SIM (m/z = 451, corresponding to the most abundant ion $[M+H]^+$ of GlaB, from 22 to 27 min) were acquired for each sample. Optimal instrument source parameters for ionization were a cone voltage of 100 V and a Probe Temperature of 550 °C [25].

MS-Quantitation. Calibration curve was built in MS in SIM mode, by monitoring the m/z = 451 corresponding to the most abundant ion $[M+H]^+$ of GlaB. Calibration standards ranged from 0.309 to 7.76 μg/mL for MS curve (y = 11655x-2890.2) with a Limit of Quantitation, LOQ, (defined for a signal-to-noise ratio > 10) of 3.09 ng on column and showing a correlation coefficient (R^2) equal to 1.

2.11. MITO-Luc mouse model treatments

Male and female MITO-Luc mice [15] (C57BL/6, aged 6–8 weeks) were injected i.p. (n = 6 for each group) with a 3:1 [100 mg/mL HP-βCD aqueous solution:ethanol] v/v mixture GlaB dissolved in the same mixture solution at increasing concentrations (from 15 up to 150 mg/kg), every second day for 18 days. The visualization of areas of cell proliferation, bioluminescence imaging and quantification of emitted light were performed as described in the literature [15].

2.12. Allograft and orthotopic Hh-MB models

Spontaneous MB from Math1-cre/$Ptc^{C/C}$ mice was isolated, minced and pipetted to obtain a single-cell suspension. Equal volumes of cells (2×10^6) were injected s.c. at the posterior flank of female BALB/c nude mice (nu/nu) (Charles River Laboratories). Tumors were grown until a median size of ~150–200 mm^3. Animals were randomly divided into six groups (n = 6/each group) and treated s.c. with a 3:1 [100 mg/mL HP-βCD aqueous solution:ethanol] v/v mixture, or cremophor solution (DMSO, 3% v/v of Cremophor, 4% v/v of Tween® 80, 15% v/v of PEG_{400}, 20 mM phosphate buffer, 0.15 M NaCl, pH 7.4), or $mPEG_{5kDa}$-cholane or GlaB (dose: 9 mg/kg) in a 3:1 [100 mg/mL HP-βCD aqueous solution:ethanol] v/v mixture, or GlaB in a cremophor solution, or loaded in $mPEG_{5KDa}$–cholane micelles. Tumor growth was monitored by measuring the size by caliper. Tumor volumes change was calculated by the formula (length × width) × 0.5 × (length + width) [14].

For orthotopic allograft model, adult female NOD/SCID (NSG) mice from Charles River Laboratories, were anesthetized by i.p. injection of ketamine (10 mg/kg) and xylazine (100 mg/kg). The posterior cranial region was shaved and placed in a stereotaxic head frame and primary cells freshly isolated from spontaneous MB of Math1-cre/$Ptc^{C/C}$ mice were stereotaxically implanted into the cerebellum (2×10^5/3 μl; at an infusion rate of 1 μl/min) according to the atlas of Franklin and Paxinos coordinates. After injection, the cannula was kept in place for 5 min and then the skin was closed over the cranioplastic assembly using metallic clips. After 14 days following tumor cells implantation, the animals were randomly divided into two groups (n = 6/each group) and treated i.v. every three days with $mPEG_{5KDa}$-cholane/GlaB (dose: 9 mg/kg) or equimolar $mPEG_{5KDa}$–cholane used as control. After 32 days of treatment, animals were sacrificed and brains were fixed in 4% formaldehyde and paraffin embedded. Tumor volume was calculated on serial 40 coronal sections of 2 μm after H&E staining of brain slice. The evaluation of tumor area of each slide was performed by a microscope (Axio Imager M1 microscope; Leica Microsystems GmbH, Wetzlar, Germany) equipped with a motorized stage and Image Pro Plus 6.2 software and the tumor volume was calculated by the formula: tumor volume = sum of measured area for each slice × slice-thickness × sampling frequency [26]. All animal experiments were approved by local ethics authorities (Ministry of Health) and conducted in accordance with Italian Governing Law (D.lgs 26/2014).

2.13. Statistical analysis

Statistical and pharmacokinetic analyses were performed as already described [27]. Briefly, the pharmacokinetic and toxicological data generated in this study were evaluated for normal distribution by use of

the Shapiro–Wilk test (SAS software, release 9.1.3; SAS Institute, Cary, NC, USA) and for homogeneity of variances using the CSS Levene test of homogeneity of variances. Since normal distribution of the data could not be rejected, comparisons were made by one-way ANOVA, via a general linear model (SAS GLM procedure). In the case of significant differences ($a = 0.05$), the ANOVA was followed by the Dunnett multiple comparisons test. For allograft and orthotopic studies, statistical analysis was performed using the StatView 4.1 software (Abacus Concepts, Berkeley, CA, USA). For all experiments, P values were determined using two-tailed Student's t-test. Unless otherwise specified, data are presented as mean ± S.D. $P < 0.05$ was considered statistically significant.

3. Results

3.1. Evaluation of toxic effects of GlaB in MITO-Luc mouse model

Preliminary *in vivo* studies were carried out to evaluate the toxicity of GlaB to non-target tissues using the recently developed transgenic reporter mouse model MITO-Luc (for mitosis luciferase). This mouse model is suitable for the non-invasive *in vivo* drug induced cell proliferation evaluation of compounds in time course experiments. The model contains a luciferase reporter under the control of an NF–Y-dependent promoter, whose activity helps in the determination of physiological and/or aberrant cell proliferation in any tissue, by bioluminescence imaging (BLI) [15]. In this study, GlaB was formulated at increasing concentrations (from 15 to 150 mg/kg) in a 3:1 [100 mg/mL 2-hydroxypropyl-β-cyclodextrin aqueous solution:ethanol] v/v mixture, a vehicle used in previous studies to evaluate the toxic effects of GlaB [14]. Fig. 1A describes the experimental protocol. MITO-Luc mice were intraperitoneally treated every second day for 18 days with GlaB or vehicle mixture only as a control. Intraperitoneal administration was selected to reproduce the treatment conditions already tested in Hh-dependent tumor models *in vivo* [14].

The BLI analysis (Fig. 1B) and the quantification of emitted light bone marrow from the femur of MITO-Luc mice in Fig. 1C, showed that GlaB did not elicit bone marrow and spleen toxicity at doses less than 50 mg/kg. A low toxic effect was observed after four injections of 100 mg/kg GlaB. The survival profiles reported in Fig. 1D do show that mortalities do not occur at doses less then 50 mg/kg, while the mortality rate at doses above 50 mg/kg increased with the dose strength.

Overall, these results indicate that GlaB does not exert toxic effects while preventing the proliferation of MB cells when used at the concentrations of 35–50 mg/kg demonstrated to inhibit *in vivo* Hh-dependent tumor growth [14].

3.2. GlaB solubility and characterization of GlaB loaded micelles

Since GlaB has poor water solubility, the preliminary GlaB solubility studies were carried out using a mixture of 2-hydroxypropyl β-cyclodextrin/ethanol (HP-βCD), which guarantees GlaB concentrations used in the study. However, this formulation includes the use of organic solvent, which should be preferably avoided in drug delivery. Therefore, HP-βCD and amphiphilic polymers, Tween® 80, Pluronic F-127, and the monomethoxy-polyethylene glycol (mPEG) derivatives, $mPEG_{5kDa}$-

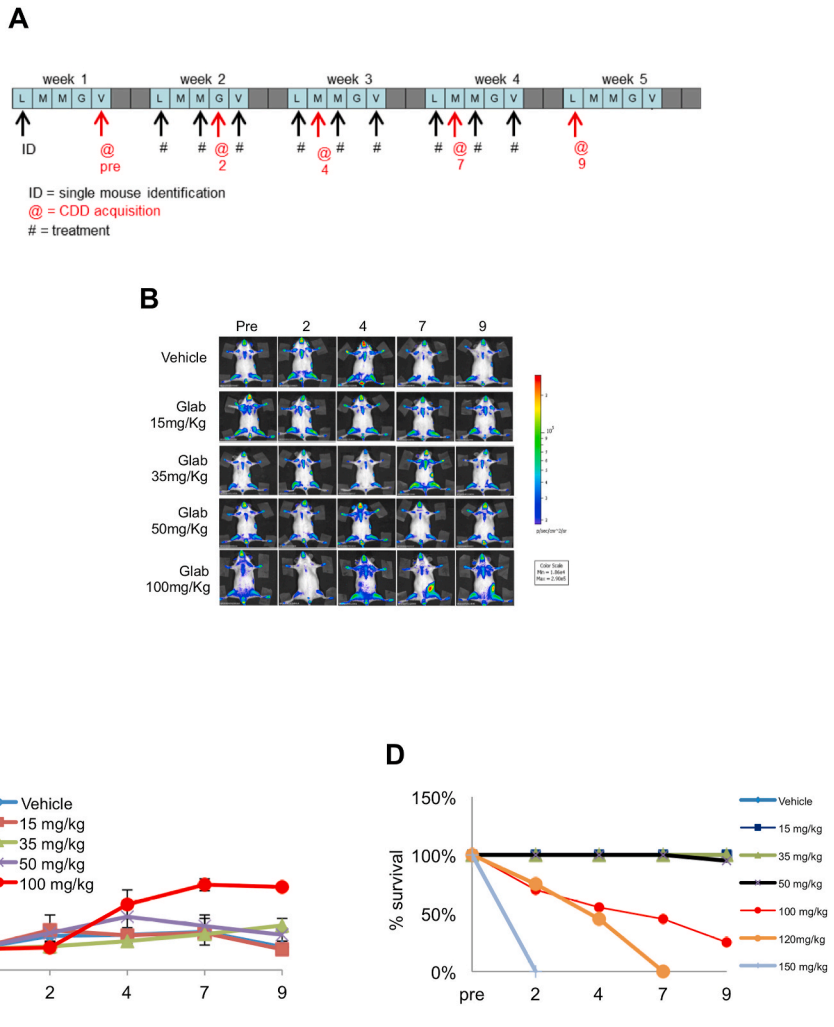

Fig. 1. Effect of GlaB on cell proliferation in MITO-Luc murine model. (A) Schematic representation of the experimental design, showing both times of treatment and imaging acquisition. (B) BLI analysis of MITO-Luc mice treated with several GlaB concentrations or with vehicle at different lifetimes after injection. (C) Quantification of emitted light bone marrow from the femur of MITO-Luc mice. The acquired bioluminescence signals in the region of interest were read out as total flux radiance (p/sec/cm^2/sr) with living Image software (Caliper Life Sciences). (D) Survival curves for MITO-Luc mice treated with different GlaB concentrations or with vehicle at different lifetimes after injection.

DSPE, $mPEG_{5kDa}$-cholane, $mPEG_{5kDa}$-cholesterol, and $mPEG_{5kDa}$-NH_2, were comparatively tested to enhance its solubility in physiological medium. HP-βCD, Tween® 80, Pluronic F-127, and $mPEG_{5kDa}$-DSPE were selected as excipients commonly used in pharmaceutical practice to increase the solubility and stability of drugs [28–32]. Additionally, $mPEG_{5kDa}$-cholane (Fig. 2A) was selected because it has recently demonstrated to remarkably enhance the biopharmaceutical properties of either small or macromolecular drugs [17,21,33]. Moreover, $mPEG_{5kDa}$-cholesterol (Fig. 2B) was used because it possesses similar chemical characteristics to that $mPEG_{5kDa}$-cholane.

The GlaB solubility profiles reported in Fig. 2C show that the ethanol free HP-βCD yielded 0.5 mM GlaB concentration (maximal solubility) at 8 mM HP-βCD concentration. The GlaB solubility decreased to 0.35 mM at higher HP-βCD concentrations (>8 mM) as a consequence of the low solubility of the GlaB/HP-βCD complex [34]. A similar effect was observed with Pluronic F-127. Tween® 80 was found to have little effect on GlaB solubility. The low capacity to increase the solubility of drugs of $mPEG_{5kDa}$-NH_2 is ascribable to its hydrophilicity, which prevents self-assembly.

$mPEG_{5kDa}$-cholane yielded the highest GlaB solubility among the amphiphilic polymers. It was observed that 1.18 mM GlaB concentration was obtained with 0.4 mM of $mPEG_{5kDa}$-cholane, corresponding a 26,000 fold GlaB concentration in water (0.02 μg/mL GlaB maximal solubility in water) [35]. Interestingly, $mPEG_{5kDa}$-cholesterol showed a lower effect than that did $mPEG_{5kDa}$-cholane on GlaB solubility despite the similarity in chemical structure.

Based on the solubility profiles, $mPEG_{5kDa}$-cholane and $mPEG_{5kDa}$-cholesterol were selected for the GlaB formulation. The GlaB encapsulation resulted in a loading capacity of $mPEG_{5kDa}$-cholane and $mPEG_{5kDa}$-cholesterol micelles of 27% and 5% w/w, respectively. Furthermore, the results reported in Fig. 2C show that the excess of these polymers does not affect the stability of the micelles and, in turn, the

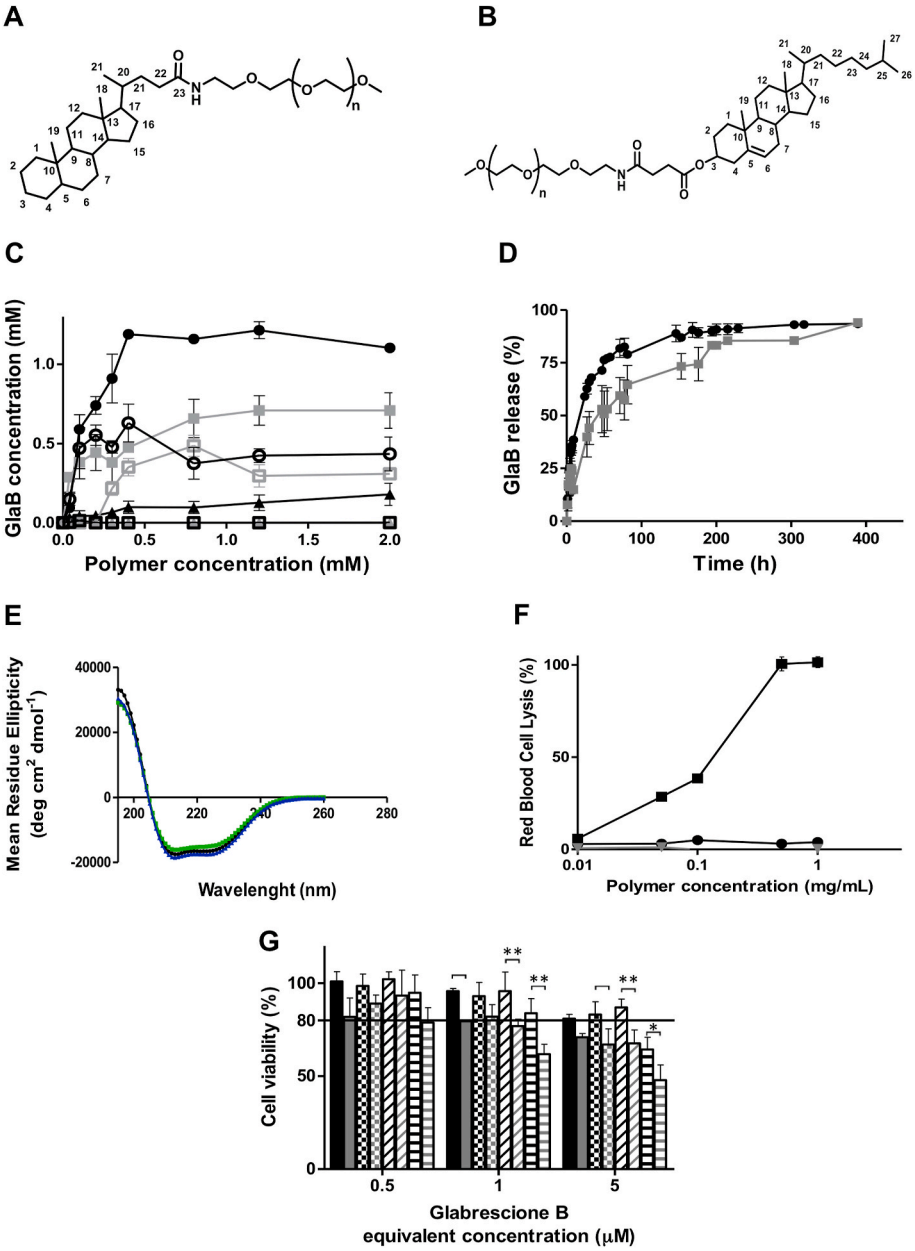

Fig. 2. Solubility and release of GlaB with micelle forming polymers and its *in vitro* biocompatibility. (A) Structure of $mPEG_{5kDa}$-cholane. (B) Structure of $mPEG_{5kDa}$-cholesterol. (C) Solubility profiles of GlaB in the presence of increasing concentrations of $mPEG_{5kDa}$-cholane (●), $mPEG_{5kDa}$-cholesterol (■), $mPEG_{5kDa}$-DSPE (▲), $mPEG_{5kDa}$-NH_2 (▲), Tween 80 (□), Pluronic F-127 (○) and HP-βCD (□) in 10 mM phosphate, 150 mM NaCl, pH 7.4. (D) GlaB cumulative release from $mPEG_{5kDa}$-cholane (●) and $mPEG_{5kDa}$-cholesterol (■) micelles in 10 mM phosphate, 150 mM NaCl, pH 7.4. (E) Circular dichroism spectra of BSA in absence (black line) and in the presence of $mPEG_{5kDa}$-cholane (green line) and $mPEG_{5kDa}$-cholesterol (blue line) micelles. (F) Hemolytic profile at increasing concentrations of $mPEG_{5kDa}$-cholane (●) and $mPEG_{5kDa}$-cholesterol (■); 10 kDa Dextran (▼) was used as biocompatible control-polymer. Data were normalized by the hemolysis observed by incubating erythrocytes with 1% v/v Triton X-100 solution (positive control). (G) Cytotoxicity profiles of Daoy cells incubated with $mPEG_{5kDa}$-cholane (black bars) and $mPEG_{5kDa}$-cholesterol (grey bars) for 12 (■), 24 (▨), 48 (▨), and 72 (▤) h. The concentration of polymers is equivalent to that of the GlaB-loaded micelles having the GlaB concentration indicated in the abscissa. Statistical analysis: *$P < 0.05$; **$P < 0.01$. (For interpretation of the references to colour in this figure legend, the reader is referred to the Web version of this article.)

drug solubility. $mPEG_{5kDa}$-cholane and $mPEG_{5kDa}$-cholesterol undergo self-assembly in water, as confirmed by their critical micelle concentrations (CMCs) which are 40.7 and 23.5 μM, respectively [18].

Size analysis by dynamic light scattering (DLS) showed homogeneous populations for both GlaB-free and GlaB-loaded formulations (PDI below 0.38). Supplementary Fig. S1A shows that the size of GlaB-free $mPEG_{5kDa}$-cholane micelles was 12.3 ± 2.3 nm, which is in conformity with results reported in the literature [17], while 16.9 ± 0.7 nm micelles were obtained with GlaB-loaded $mPEG_{5kDa}$-cholane. Supplementary Fig. S1B shows that in the case of $mPEG_{5kDa}$-cholesterol, the GlaB-free and GlaB-loaded micelles had sizes of 17.9 ± 0.3 and 21.7 ± 0.7 nm, respectively.

The TEM images reported in Supplementary Figs. S1C and S1D show that all the GlaB-free and GlaB-loaded micelles obtained with $mPEG_{5kDa}$-cholane and GlaB-loaded $mPEG_{5kDa}$-cholesterol had a typical spherical micelle shape, and the dimensional data were in conformity with the DLS results. The TEM images also showed that the encapsulation of the GlaB did not affect the conformation of the micelles.

The GlaB-loaded $mPEG_{5kDa}$-cholane and GlaB-loaded $mPEG_{5kDa}$-cholesterol micelles remained colloidally stable over a period of four weeks (Supplementary Fig. S1E). The stability of the GlaB-loaded $mPEG_{5kDa}$-cholane and GlaB-loaded $mPEG_{5kDa}$-cholesterol micelles was further investigated after a freeze-thaw cycle. The results showed that the size of the GlaB-loaded micelles was comparable to that of the freshly prepared formulations (Supplementary Fig. S2).

GlaB release from $mPEG_{5kDa}$-cholane and $mPEG_{5kDa}$-cholesterol micelles in 10 mM phosphate and 150 mM NaCl (PBS), buffer at pH 7.4 was carried out to mimic the release under physiological conditions. Fig. 2D shows that the release of GlaB was slightly faster from $mPEG_{5kDa}$-cholane micelles than from $mPEG_{5kDa}$-cholesterol micelles. In the first 24 h, 59% and 35% of GlaB were released from $mPEG_{5kDa}$-cholane and $mPEG_{5kDa}$-cholesterol micelles, respectively. In both cases, 95% of GlaB was released in 400 h.

3.3. Micelle biocompatibility

Due to their amphiphilic character, $mPEG_{5kDa}$-cholane and $mPEG_{5kDa}$-cholesterol may affect the protein stability and the integrity of cell membranes resulting in poor biocompatibility. Association with amphiphilic polymers can in fact induce structural protein changes yielding biological inactivation and toxicity [36], while cell membrane association can result in hemolysis and cytotoxicity. Changes of structure of bovine serum albumin (BSA) upon exposure to the micelles were evaluated as a model. The results reported in Fig. 2E show that BSA maintains its typical α-helix conformation when exposed to $mPEG_{5kDa}$-cholane and $mPEG_{5kDa}$-cholesterol micelles, with negligible conformational changes. The slight α-helix decrease (61.4% and 63.7% for $mPEG_{5kDa}$-cholane and $mPEG_{5kDa}$-cholesterol micelles, respectively) compared to that of BSA in plain buffer (i.e., 65.7%) [37] was correlated to a slight increase in β-sheet and random coil structure (Supplementary Fig. S3).

Fig. 2Fshows the hemolytic activity resulting from incubation of $mPEG_{5kDa}$-cholane and $mPEG_{5kDa}$-cholesterol with mouse erythrocytes. At the highest concentration, the hemolysis induced by $mPEG_{5kDa}$-cholane was 3.9 ± 0.1%, which is below the threshold (5%) reported by the Guiding Principles of Hemolysis Test [H]GPT4-1 for nanocarrier toxicity [38]. $mPEG_{5kDa}$-cholesterol showed remarkable cell membrane disruption under the tested conditions (100 ± 2.3%) compared to $mPEG_{5kDa}$-cholane, which is attributable to the different chemical structures of the two amphiphilic polymers.

Fig. 2Gshows that the cytotoxicity of both materials was time and concentration-dependent in human MB Daoy cells. However, $mPEG_{5kDa}$-cholane appeared to be significantly less toxic than $mPEG_{5kDa}$-cholesterol.

To elucidate the ability of $mPEG_{5kDa}$-cholane and $mPEG_{5kDa}$-cholesterol to trigger inflammatory signals, the production of mRNA encoding for two inflammatory cytokines, namely TNFα and IL-6, by PBMCs was evaluated. LPS was used as a positive control. Supplementary Figs. S4A and S4C show that both $mPEG_{5kDa}$-cholesterol and $mPEG_{5kDa}$-cholane did not boost the production of mRNA encoding for TNF-α or TNF-α release. SupplementaryFigs. S4B and S4D show that $mPEG_{5kDa}$-cholesterol does not boost IL-6 encoding mRNA production or IL-6 release. In the case of $mPEG_{5kDa}$-cholane, only the highest polymer concentration (3 μM) elicited a significant increase in IL-6 mRNA expression ($p < 0.001$) and IL-6 release, which was consistent with the mRNA expression.

3.4. Effect of $mPEG_{5kDa}$-cholane/GlaB formulation on GLI1-dependent MB growth and Hh signaling activity in vitro

The effect of GlaB-loaded $mPEG_{5kDa}$-cholane and GlaB-loaded $mPEG_{5kDa}$-cholesterol micelles on Hh-dependent tumor cell growth was evaluated using freshly isolated primary tumor cells from Math1-cre/$Ptc^{C/C}$ mice, which spontaneously develop MB [14,19,39].

Fig. 3A–C shows that GlaB-free $mPEG_{5kDa}$-cholane micelles did not affect cell proliferation or cell death (Supplementary Fig. S5). Conversely, GlaB-free $mPEG_{5kDa}$-cholesterol micelles demonstrated an unspecified decrease in primary MB cell proliferation (Supplementary Figs. S6A-C) due to cell death (Supplementary Figs. S6D-F), which is in agreement with the cytotoxicity data reported above (Fig. 2G). Furthermore, GlaB-loaded $mPEG_{5kDa}$-cholane formulation was more effective for proliferation inhibition, even at low concentrations (0.5 and 1 μM), than unformulated GlaB. Importantly, the inhibition of cell proliferation correlates with a significant decrease in Hh-target gene mRNA expression levels, such as *Gli1* and *CycD2* levels (Fig. 3D and E).

Given that $mPEG_{5kDa}$-cholesterol micelles showed significant cell membrane toxicity, tested by hemolysis assays (Fig. 2F), and unspecified toxic effects on the proliferation of Hh-dependent tumor cells (Fig. 2G and Supplementary Fig. S6), this polymeric nanocarrier was excluded from the following *in vitro* and *in vivo* biological evaluations.

To prove the direct inhibitory effect of GlaB encapsulated in $mPEG_{5kDa}$-cholane micelles on Hh signaling, we determined its effect on GLI1 transcription function. To this end, we treated mouse embryonic fibroblasts (MEFs) transiently expressing ectopic GLI1 and a GLI-dependent luciferase reporter with increasing concentrations of $mPEG_{5kDa}$-cholane/GlaB formulation. As shown in Fig. 3F, GlaB encapsulated in micelles strongly inhibited GLI1 transcriptional activity at much lower concentrations (IC_{50} = 0.48 μM) than that previously reported for GlaB (IC_{50} = 12 μM) [14]. Moreover, no modulation of Renilla, used as an internal control of the transcriptional assay, has been shown for both GlaB-free $mPEG_{5kDa}$-cholane and $mPEG_{5kDa}$-cholane/-GlaB, underscoring the non-toxicity of the formulations to cells.

3.5. Pharmacokinetic study of $mPEG\text{-}cholane_{5kDa}$/GlaB formulation

The pharmacokinetic (PK) profile of GlaB formulated with $mPEG_{5kDa}$-cholane micelles after intravenous administration was investigated in c57BL/6 mice. This mouse strain was selected because it is commonly used for PK studies for colloidal formulations of drugs [40,41]. GlaB dissolved in non-ionic surfactant/DMSO (non-formulated GlaB), a mixture commonly used to administer insoluble drugs in preclinical studies [42], was also administered as a control.

Fig. 3G and Table 1 show that the GlaB loaded in $mPEG_{5kDa}$-cholane micelles and non-formulated GlaB have similar PK profiles, both fitting a biexponential profile. The PK analysis indicated that $mPEG_{5kDa}$-cholane did not significantly affect the circulation time of GlaB. However, a slight increase in the elimination half-life ($t_{1/2\beta}$) and the area under the *concentration-vs-time curve* ($AUC_{0\text{-}inf}$), and a decrease in the clearance (CL) were observed for GlaB formulated with $mPEG_{5kDa}$-cholane micelles compared to those in the non-formulated GlaB, suggesting that the $mPEG_{5kDa}$-cholane formulation can slightly affect the circulation time of this molecule.

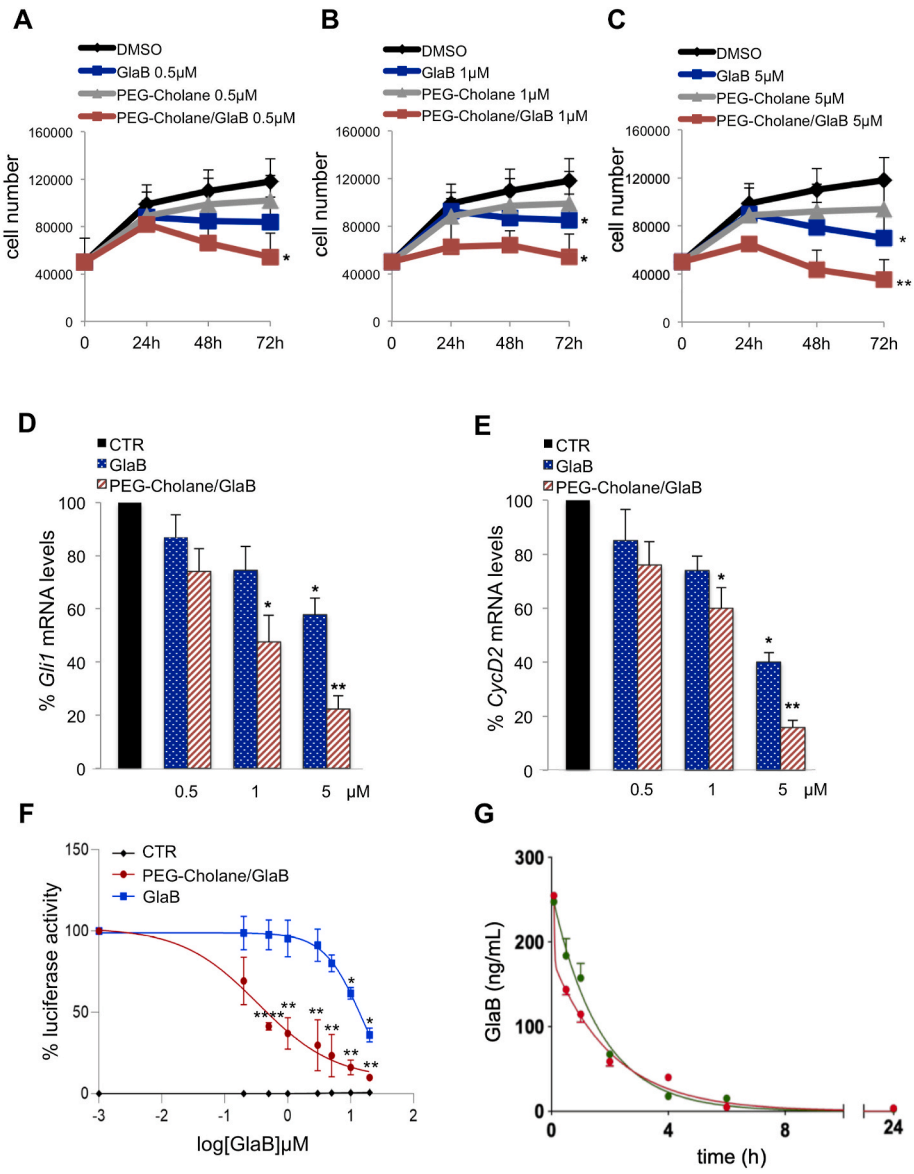

Fig. 3. mPEG$_{5kDa}$-cholane/GlaB formulation affects the *in vitro* proliferation of Hh-dependent primary MB cells and GLI1 transcriptional activity. (A–C) Primary MB cell cultures from Math1-cre/Ptc$^{C/C}$ mice were treated with GlaB or mPEG$_{5KDa}$-cholane/GlaB (0.5, 1, and 5 μM) and control vehicles. After the indicated times, a trypan blue count was performed to determine the growth rate of viable cells. (D and E) *Gli1* and *CyclinD2* mRNA expression levels were determined by qRT-PCR normalized to endogenous controls (*β2-microglobulin* and *HPRT*). (F) Inhibition of GLI1-induced transcription was assessed in MEFs transfected with 12XGliBS-Luc and pRL-TK Renilla (normalization control) plus control (empty) or GLI1 vector and treated with increasing concentrations of mPEG$_{5kDa}$-cholane/GlaB for 24 h. All data show the mean ± S.D. of three independent experiments. *P < 0.05; **P < 0.01; ****P < 0.0001 versus CTR. (G) Pharmacokinetic profiles of GlaB and GlaB-loaded micelles in mice. Mean plasma concentration-time profile of GlaB after i.v. administration of a single dose of GlaB (2.5 mg/kg) in a control vehicle (● red) and mPEG$_{5kDa}$-cholane (● green) micelles to c57BL/6 mice (n = 4). Data are presented as mean ± SEM. (For interpretation of the references to colour in this figure legend, the reader is referred to the Web version of this article.)

Table 1
Pharmacokinetic parameters of GlaB.

	Parameter			
Formulation	**$t_{1/2\beta}$ (h)**	**V_β (L/Kg)**	**CL (L/h•Kg)**	**$AUC_{0\text{-}inf}$ (ng/mL•h)**
mPEG$_{5kDa}$-cholane/GlaB	1.90 ± 0.64	10.93 ± 5.12	3.984 ± 0.934	627 ± 245
GlaB in surfactant/DMSO	1.61 ± 0.78	14.01 ± 4.52	6.019 ± 1.564	415 ± 123

3.6. *Effect of mPEG$_{5kDa}$-cholane/GlaB formulation on GLI1-dependent MB growth in vivo*

To further assess the therapeutic efficacy of mPEG$_{5kDa}$-cholane/GlaB in an *in vivo* model of Hh-dependent tumors, GlaB-loaded mPEG$_{5kDa}$-cholane micelles were administered to nude mice posterior flank grafted with primary MB cells freshly isolated from Math1-cre/Ptc$^{C/C}$ mice. The mice were treated subcutaneously with 9 mg/kg (n = 6 for each group) GlaB encapsulated in mPEG$_{5kDa}$-cholane micelles daily. For comparison, 9 mg/kg (n = 6 for each group) GlaB dissolved in a 3:1 [100 mg/mL HP-βCD aqueous solution:ethanol] v/v mixture or in a mixture containing 3.3% DMSO, 3% cremophor, 4% Tween®80, 15% PEG 400, 74.7% PBS, pH 7.4 were used. GlaB-free vehicles were used as controls. GlaB-loaded mPEG$_{5kDa}$-cholane reduced tumor growth rate and tumor volume (at the end point of experiment, Fig. 4K and L) than that did GlaB dissolved in the 2-HP-βCD/ethanol mixture (Fig. 4A and B) and GlaB dissolved in the cremophor/DMSO containing mixture (Fig. 4F and G). Accordingly, Fig. 4M–O shows that GLI1 mRNA and protein levels, known readout of Hh signaling, and percentage of positive cells to the proliferation marker Ki67, were drastically reduced in mice treated with GlaB-loaded mPEG$_{5kDa}$-cholane based formulation than in mice treated with control GlaB formulations (Fig. 4C–E and 4H-J). Similarly, the expression of other Hh target genes (*CycD2*, *Gli2,* and *Ptch1*) was strongly reduced in GlaB-loaded mPEG$_{5kDa}$-cholane treated mice than in GlaB formulations-treated mice (Supplementary Fig. S7).

Overall, these findings suggest that GlaB encapsulated in mPEG$_{5kDa}$-cholane micellar colloidal system provides a greater inhibition of Hh-dependent tumor growth than that in control GlaB formulations. It is worth noting that the cell proliferation inhibition data (tumor volume growth, GLI1 mRNA and protein levels, and Ki67 labeling, Fig. 4K-O) showed a statistically significant difference between the mPEG$_{5kDa}$-cholane micellar formulation and the free drug vehicles, while no

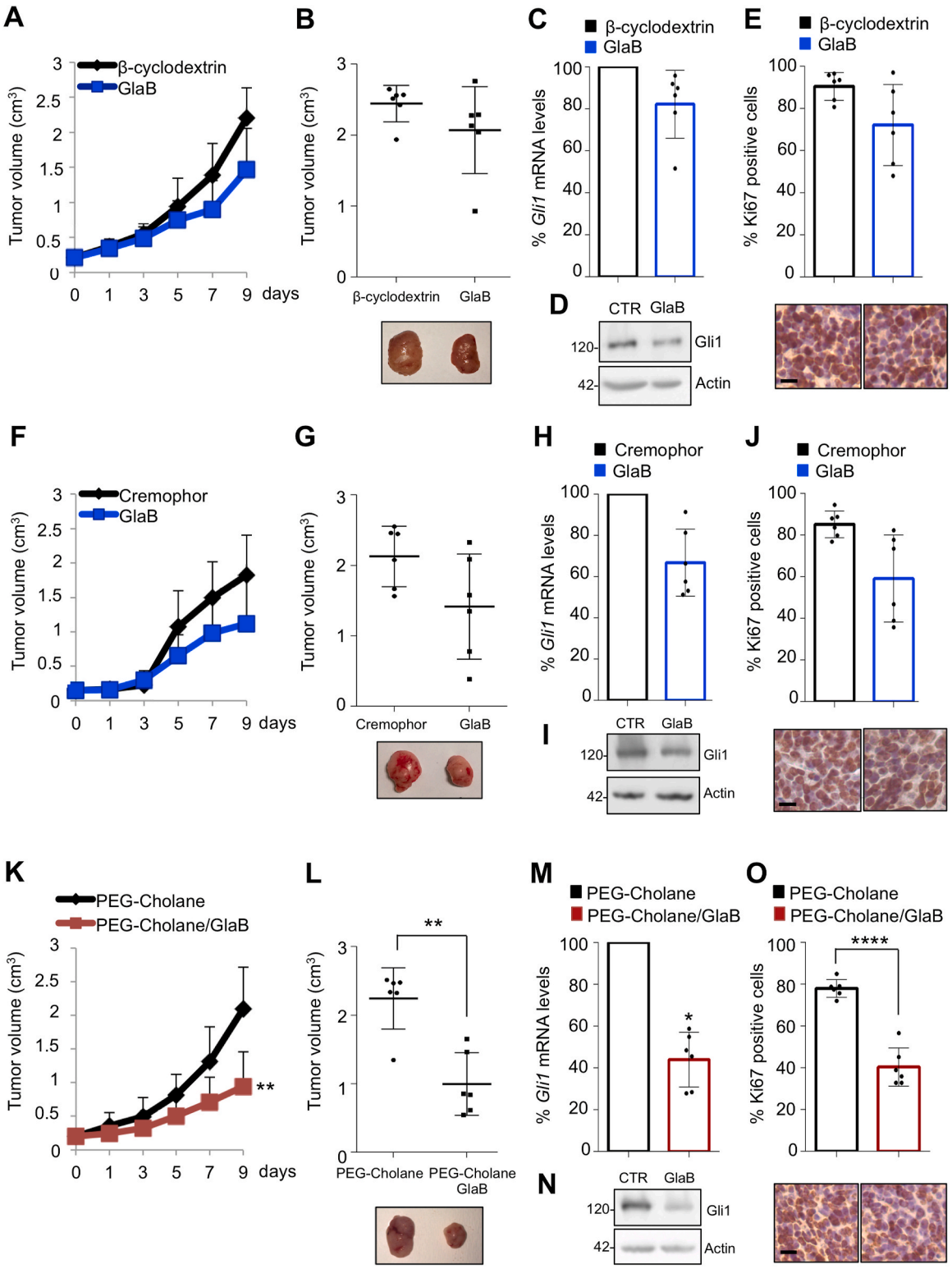

Fig. 4. mPEG$_{5kDa}$-cholane/GlaB formulation affects the *in vivo* Hh-dependent MB tumor growth. (A, F, and K) Change of tumor volume during the period of treatment. Nu/nu mice (n = 6 for each group) were grafted with spontaneous primary MB from Math1-cre/Ptc$^{C/C}$ mice. Tumor masses (150–200 mm^3) were treated with GlaB dissolved in a 2-HP-βCD/ethanol mixture (A), GlaB dissolved in a cremophor/DMSO mixture (F), mPEG$_{5kDa}$-cholane/GlaB formulation (K), or respective vehicles as control. Tumor growth was monitored by caliper every second day. (B, G, and L) Representative flank allograft average volumes (lower panel) and quantification of tumor explants (upper panel). (C, H and M) *Gli1* mRNA expression levels of MB tumor masses treated with GlaB in 2-HP-βCD/ethanol and cremophor/DMSO mixtures (C and H) or mPEG$_{5kDa}$-cholane/GlaB formulation (M) were determined by qRT-PCR normalized to endogenous controls (*β2-microglobulin* and *HPRT*). (D, I, and N) Gli1 protein levels of MB tumor samples treated with GlaB in 2-HP-βCD/ethanol and cremophor/DMSO mixtures (D and I) or mPEG$_{5kDa}$-cholane/GlaB formulation (N) were determined by immunoblot analysis. Actin was used as a loading control. (E, J, and O) Immunohistochemical staining of Ki67 (lower panel) and its quantification in allograft tumor samples treated with GlaB in 2-HP-βCD/ethanol and cremophor/DMSO mixtures (E and J) or mPEG$_{5kDa}$-cholane/GlaB formulation (O). Scale bars represent 10 μm for Ki67. Error bars indicate S.D. *P < 0.05; **P < 0.01; ****P < 0.0001 versus CTR.

statistically significant difference was observed between the other drug formulations and the free drug vehicles.

3.7. GlaB loaded in mPEG$_{5kDa}$-cholane micelles crosses the BBB and inhibits tumor growth in a Hh-dependent MB orthotopic model

To investigate the delivery of GlaB encapsulated in mPEG$_{5kDa}$-cholane micelles, its concentration in the brain and cerebellum of GlaB-treated mice was measured by HPLC coupled with Electrospray Mass Spectrometry (HPLC-MS). To achieve this aim, CD1 wild-type mice were i.v. injected with mPEG$_{5kDa}$-cholane/GlaB formulation (dose: 9 mg/kg) at four different time points: 30 min, 1, 2, and 4 h after which the brain and cerebellum extracts were analyzed using HPLC-MS analysis. The results obtained were elaborated as the percentage of injected dose per gram of organ (%ID/g of organ). Fig. 5A shows that the percentage of GlaB was 1.93% ID/g in the brain and 1.87% ID/g in the cerebellum 1 h after administration. Two hours later, a reduction in GlaB percentage values corresponding to 1.8% ID/g of brain and 1.67% ID/g of the cerebellum was observed. The percentage of GlaB associated with the brain and cerebellum at 30 min and 4 h was lower than LOQ concentration of 0.309 μg/mL.

The ability of GlaB encapsulated in mPEG$_{5kDa}$-cholane micelles to cross the blood-brain barrier (BBB) and biodistribute in the brain and cerebellum, as observed in the HPLC-MS, was confirmed in an orthotopic model of Hh-dependent MB. Primary MB cells were implanted into the cerebellum of NOD/SCID mice and randomly divided into two groups and intravenously injected with mPEG$_{5kDa}$-cholane/GlaB formulation (dose: 9 mg/kg) or GlaB-free mPEG$_{5kDa}$-cholane. Fig. 5B and C shows that after treatment, the tumor volume underwent a significant reduction in GlaB loaded mPEG$_{5kDa}$-cholane micelles compared to control. Fig. 5B and D shows that the inhibition of tumor growth in treated mice was correlated with a decreased percentage of Ki67 positive cells.

4. Discussion

MB is a pediatric malignancy that is responsible for significant morbidity and mortality. Currently, MB patients have very poor prognosis, and efficacious and safe therapies are not available. The standard of care treatment of MB is surgery followed by chemotherapy and/or radiotherapy, which often results in severe cognitive defects and permanent disabilities in surviving patients. Multi-omics data highlighted the high heterogeneity of this tumor, leading to the identification of twelve molecular subtypes with distinct genetic and clinical features [43]. Although the Hh-MB subgroup has a favorable treatment outcome, the risk assessment is highly dependent on the genomic profile and the

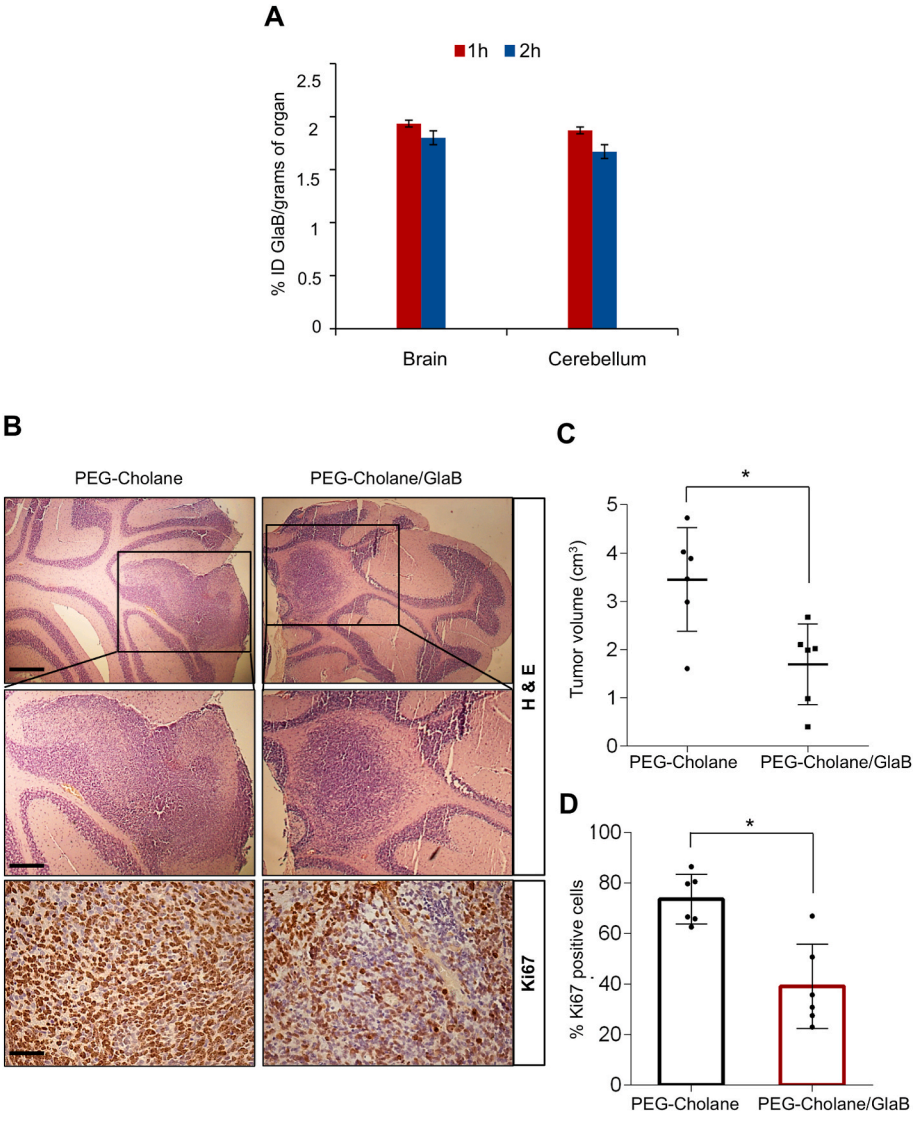

Fig. 5. Biodistribution in the brain and the cerebellum of GlaB encapsulated in mPEG$_{5kDa}$-cholane micelles and its effects in an orthotopic model of Hh-dependent MB. (A) Representative histograms show percentage of injected dose per gram of organ (%ID/g of organ) at 1 h and 2 h after i.v. administration of mPEG$_{5kDa}$-cholane/GlaB formulation (9 mg/kg). Data were expressed as means ± S.D. (n = 2). ID: Injected dose. (B) Representative H&E images (low and high magnification) of a murine MB cell-derived orthotopic tumor in NSG mice after i.v. injection of mPEG$_{5kDa}$-cholane/GlaB formulation or vehicle only. Scale bars represent 500 μm (upper panels) and 250 μm (lower panels) for H&E staining and 100 μm for Ki67 staining. (C) Representative tumor average volumes after explantation. (D) Quantification of Ki67 stainings from immunohistochemistry shown in (B). Error bars indicate S.D. *P < 0.05 versus CTR.

age of the patients. Hence, treatment of Hh-MB remains a challenge in pediatric tumor biology. To date, innovative therapies have been investigated using drugs able to modulate the Hh pathway at both upstream and downstream levels. FDA-approved SMO antagonists (i.e., vismodegib, sonidegib, and glasdegib), although well tolerated in adult patients, induce developmental bone abnormalities in young mice [44], and are therefore not recommended for use in children. Furthermore, SMO inhibitors induce early resistance and are ineffective in tumors harboring mutations in Hh pathway genes downstream of SMO. GLI1 inhibitors, such as GANT61 and ATO, despite their peculiar selectivity and therapeutic potential, have not been studied in clinical trials for MB patients, most likely due to their limited potency and low BBB permeability [45–48]. In this context, our study shows that the $mPEG_{5kDa}$-cholane/GlaB micellar system can be properly exploited in the treatment of patients with Hh-MB, particularly for those tumors showing resistance to SMO inhibitors or harboring GLI1 hyperactivation by SMO-independent mechanisms. The results reported in this work show that pharmacokinetic drawbacks due to the poor solubility of GlaB can be overcome by using micelle-forming amphiphilic polymers. Accordingly, $mPEG_{5kDa}$-cholane was found to increase GlaB solubility up to about 0.5 mg/mL, a suitable concentration for parenteral administration in the clinical setting. This formulation avoids the use of organic solvents or pharmaceutical excipients commonly used to solubilize poorly soluble drugs, because they may elicit toxic effects, such as cremophor. $mPEG_{5kDa}$-cholane and $mPEG_{5kDa}$-cholesterol possess similar polycyclic molecules at one end of the mPEG chain (Fig. 2A and B); however, the polycyclic molecules is inverted in these two derivatives. The different orientations of the polycyclic moieties may induce different arrangements in the core of $mPEG_{5kDa}$-cholane and $mPEG_{5kDa}$-cholesterol micelles, which can result in different GlaB encapsulation and solubility, as observed in the release profile of GlaB from the two colloidal systems in this study. The structural features of the two amphiphilic polymers investigated in this study had a correlation with their biocompatibility as observed in the cytotoxicity tests performed on erythrocytes and Daoy cells. The lower biocompatibility of $mPEG_{5kDa}$-cholesterol compared to $mPEG_{5kDa}$-cholane may also be attributed to their different conformations as different orientations of the polycyclic moieties affect their interaction with the cell membrane and the dissolution of cell membrane components. Furthermore, $mPEG_{5kDa}$-cholane did not elicit pro-inflammatory cytokines at therapeutic concentrations, further confirming its biocompatibility.

In an *in vitro* MB model, $mPEG_{5kDa}$-cholane micelles have been found to enhance GlaB diffusion through the cell membrane. The encapsulation of GlaB in $mPEG_{5kDa}$-cholane-based micelles also provided a slight improvement in the pharmacokinetic profile. Conceivably, the micelles may undergo dissociation when diluted in the blood and when exposed to biological components (i.e., blood cells, vessel endothelium surface, blood circulating proteins), thus retaining the GlaB and modulating its fate. We hypothesize that after micelle release in the blood, GlaB binds plasmatic proteins, albumin in particular, as it occurs with several hydrophobic drugs such as Paclitaxel [49]. The enhanced GlaB solubility by $mPEG_{5kDa}$-cholane is advantageous as it facilitates the biodistribution of the drug to intracranial tumors resulting in therapeutic efficacy. Furthermore, the subcutaneous administration of the GlaB-loaded/$mPEG_{5kDa}$-cholane micelles enhanced the therapeutic activity compared to GlaB administered with 2-HP-βCD/ethanol or with cremophor/DMSO containing mixtures, which may be due to a higher $mPEG_{5kDa}$-cholane micelles bioavailability than that in the other formulations.

The promising pharmacokinetic properties and low toxicity also indicate that GlaB encapsulated in $mPEG_{5kDa}$-cholane micelles is a potential treatment option for patients with Hh-MB, particularly for those who present SMO downstream mutations or relapse after SMO inhibitor treatment.

Authors' contributions

Paola Infante: investigation, validation, data curation, writing original draft, **Alessio Malfanti**: investigation, validation, data curation, **Deborah Quaglio**: investigation, validation, data curation, **Silvia Balducci**: investigation, formal analysis, **Sara De Martin**: investigation, methodology, writing original draft, **Francesca Bufalieri**: investigation, formal analysis, **Francesca Mastrotto**: investigation, **Irene Basili**: investigation, **Mariangela Garofalo**: investigation, **Ludovica Lospinoso Severini**: investigation, **Mattia Mori**: validation, formal analysis, **Isabella Manni**: investigation, formal analysis, **Marta Moretti**: investigation, **Carmine Nicoletti**: investigation, **Giulia Piaggio**: methodology, data curation, **Paolo Caliceti**: writing original draft, editing, **Bruno Botta**: methodology, supervision, writing original draft, **Francesca Ghirga**: supervision, writing original draft, **Stefano Salmaso**: conceptualization, supervision, funding acquisition, writing original draft, **Lucia Di Marcotullio**: conceptualization, supervision, funding acquisition, project administration, writing original draft.

Acknowledgements

This work was supported by Associazione Italiana per la Ricerca sul Cancro Grants #IG20801; Progetti di Ricerca di Università Sapienza di Roma; Italian Ministry of Education, University and Research (MIUR) Grants PRIN 2017BF3PXZ and 20175XBSX4; Dipartimenti di Eccellenza - L. 232/2016; Pasteur Institute/Cenci Bolognetti Foundation; Istituto Italiano di Tecnologia (IIT).

Appendix A. Supplementary data

Supplementary data to this article can be found online at https://doi.org/10.1016/j.canlet.2020.11.028.

Declaration of competing InterestCOI

The authors declare that they have no known competing financial interests or personal relationships that could have appeared to influence the work reported in this paper.

References

[1] F. Wu, Y. Zhang, B. Sun, A.P. McMahon, Y. Wang, Hedgehog signaling: from basic biology to cancer therapy, Cell Chem Biol 24 (2017) 252–280.
[2] J. Wang, A. Garancher, V. Ramaswamy, R.J. Wechsler-Reya, Medulloblastoma: from molecular subgroups to molecular targeted therapies, Annu. Rev. Neurosci. 41 (2018) 207–232.
[3] V. Hovestadt, O. Ayrault, F.J. Swartling, G.W. Robinson, S.M. Pfister, P. A. Northcott, Medulloblastomics revisited: biological and clinical insights from thousands of patients, Nat. Rev. Canc. 20 (2020) 42–56.
[4] L. Lospinoso Severini, F. Ghirga, F. Bufalieri, D. Quaglio, P. Infante, L. Di Marcotullio, The SHH/GLI signaling pathway: a therapeutic target for medulloblastoma, Expert Opin. Ther. Targets (2020) 1–23.
[5] C.C. Hui, S. Angers, Gli proteins in development and disease, Annu. Rev. Cell Dev. Biol. 27 (2011) 513–537.
[6] M. Sabol, D. Trnski, V. Musani, P. Ozretić, S. Levanat, Role of GLI transcription factors in pathogenesis and their potential as new therapeutic targets, Int. J. Mol. Sci. 19 (2018).
[7] M.E. Hutchin, M.S. Kariapper, M. Grachtchouk, A. Wang, L. Wei, D. Cummings, J. Liu, L.E. Michael, A. Glick, A.A. Dlugosz, Sustained Hedgehog signaling is required for basal cell carcinoma proliferation and survival: conditional skin tumorigenesis recapitulates the hair growth cycle, Genes Dev. 19 (2005) 214–223.
[8] S.J. Scales, F.J. de Sauvage, Mechanisms of Hedgehog pathway activation in cancer and implications for therapy, Trends Pharmacol. Sci. 30 (2009) 303–312.
[9] S. Pietrobono, S. Gagliardi, B. Stecca, Non-canonical Hedgehog signaling pathway in cancer: activation of GLI transcription factors beyond smoothened, Front. Genet. 10 (2019) 556.
[10] P. Infante, R. Alfonsi, B. Botta, M. Mori, L. Di Marcotullio, Targeting GLI factors to inhibit the Hedgehog pathway, Trends Pharmacol. Sci. 36 (2015) 547–558.
[11] D. Quaglio, P. Infante, L. Di Marcotullio, B. Botta, M. Mori, Hedgehog signaling pathway inhibitors: an updated patent review (2015-present), Expert Opin. Ther. Pat. 30 (2020) 235–250.
[12] C. Wang, H. Wu, T. Evron, E. Vardy, G.W. Han, X.P. Huang, S.J. Hufeisen, T. J. Mangano, D.J. Urban, V. Katritch, V. Cherezov, M.G. Caron, B.L. Roth, R.

C. Stevens, Structural basis for Smoothened receptor modulation and chemoresistance to anticancer drugs, Nat. Commun. 5 (2014) 4355.
[13] J. Briscoe, P.P. Thérond, The mechanisms of Hedgehog signalling and its roles in development and disease, Nat. Rev. Mol. Cell Biol. 14 (2013) 416–429.
[14] P. Infante, M. Mori, R. Alfonsi, F. Ghirga, F. Aiello, S. Toscano, C. Ingallina, M. Siler, D. Cucchi, A. Po, E. Miele, D. D'Amico, G. Canettieri, E. De Smaele, E. Ferretti, I. Screpanti, G. Uccello Barretta, M. Botta, B. Botta, A. Gulino, L. Di Marcotullio, Gli1/DNA interaction is a druggable target for Hedgehog-dependent tumors, EMBO J. 34 (2015) 200–217.
[15] F. Goeman, I. Manni, S. Artuso, B. Ramachandran, G. Toietta, G. Bossi, G. Rando, C. Cencioni, S. Germoni, S. Straino, M.C. Capogrossi, S. Bacchetti, A. Maggi, A. Sacchi, P. Ciana, G. Piaggio, Molecular imaging of nuclear factor-Y transcriptional activity maps proliferation sites in live animals, Mol. Biol. Cell 23 (2012) 1467–1474.
[16] S. Salmaso, S. Bersani, F. Mastrotto, G. Tonon, R. Schrepfer, S. Genovese, P. Caliceti, Self-assembling nanocomposites for protein delivery: supramolecular interactions between PEG-cholane and rh-G-CSF, J. Contr. Release 162 (2012) 176–184.
[17] E. Ambrosio, M. Barattin, S. Bersani, S. Shubber, S. Uddin, C.F. van der Walle, P. Caliceti, S. Salmaso, A novel combined strategy for the physical PEGylation of polypeptides, J. Contr. Release 226 (2016) 35–46.
[18] F. Mastrotto, C. Brazzale, F. Bellato, S. De Martin, G. Grange, M. Mahmoudzadeh, A. Magarkar, A. Bunker, S. Salmaso, P. Caliceti, In vitro and in vivo behavior of liposomes decorated with PEGs with different chemical features, Mol. Pharm. 17 (2020) 472–487.
[19] S. Berardozzi, F. Bernardi, P. Infante, C. Ingallina, S. Toscano, E. De Paolis, R. Alfonsi, M. Caimano, B. Botta, M. Mori, L. Di Marcotullio, F. Ghirga, Synergistic inhibition of the Hedgehog pathway by newly designed Smo and Gli antagonists bearing the isoflavone scaffold, Eur. J. Med. Chem. 156 (2018) 554–562.
[20] A.D. Bangham, M.M. Standish, J.C. Watkins, Diffusion of univalent ions across the lamellae of swollen phospholipids, J. Mol. Biol. 13 (1965), 238-IN227.
[21] C. Luengo-Alonso, J.J. Torrado, M.P. Ballesteros, A. Malfanti, S. Bersani, S. Salmaso, P. Caliceti, A novel performing PEG-cholane nanoformulation for Amphotericin B delivery, Int. J. Pharm. 495 (2015) 41–51.
[22] D. Polyak, A. Krivitsky, A. Scomparin, S. Eliyahu, H. Kalinski, S. Avkin-Nachum, R. Satchi-Fainaro, Systemic delivery of siRNA by aminated poly(α)glutamate for the treatment of solid tumors, J. Contr. Release 257 (2017) 132–143.
[23] M. Kool, D.T. Jones, N. Jäger, P.A. Northcott, T.J. Pugh, V. Hovestadt, R.M. Piro, L. A. Esparza, S.L. Markant, M. Remke, T. Milde, F. Bourdeaut, M. Ryzhova, D. Sturm, E. Pfaff, S. Stark, S. Hutter, H. Seker-Cin, P. Johann, S. Bender, C. Schmidt, T. Rausch, D. Shih, J. Reimand, L. Sieber, A. Wittmann, L. Linke, H. Witt, U. D. Weber, M. Zapatka, R. König, R. Beroukhim, G. Bergthold, P. van Sluis, R. Volckmann, J. Koster, R. Versteeg, S. Schmidt, S. Wolf, C. Lawerenz, C. C. Bartholomae, C. von Kalle, A. Unterberg, C. Herold-Mende, S. Hofer, A. E. Kulozik, A. von Deimling, W. Scheurlen, J. Felsberg, G. Reifenberger, M. Hasselblatt, J.R. Crawford, G.A. Grant, N. Jabado, A. Perry, C. Cowdrey, S. Croul, G. Zadeh, J.O. Korbel, F. Doz, O. Delattre, G.D. Bader, M.G. McCabe, V. P. Collins, M.W. Kieran, Y.J. Cho, S.L. Pomeroy, O. Witt, B. Brors, M.D. Taylor, U. Schüller, A. Korshunov, R. Eils, R.J. Wechsler-Reya, P. Lichter, S.M. Pfister, I.P. T. Project, Genome sequencing of SHH medulloblastoma predicts genotype-related response to smoothened inhibition, Canc. Cell 25 (2014) 393–405.
[24] P. Palatini, S. De Martin, Pharmacokinetic drug interactions in liver disease: an update, World J. Gastroenterol. 22 (2016) 1260–1278.
[25] G. D'Alessandro, D. Quaglio, L. Monaco, C. Lauro, F. Ghirga, C. Ingallina, M. De Martino, S. Fucile, A. Porzia, M.A. Di Castro, F. Bellato, F. Mastrotto, M. Mori, P. Infante, P. Turano, S. Salmaso, P. Caliceti, L. Di Marcotullio, B. Botta, V. Ghini, C. Limatola, H-NMR metabolomics reveals the Glabrescione B exacerbation of glycolytic metabolism beside the cell growth inhibitory effect in glioma, Cell Commun. Signal. 17 (2019) 108.
[26] F. Bufalieri, P. Infante, F. Bernardi, M. Caimano, P. Romania, M. Moretti, L. Lospinoso Severini, J. Talbot, O. Melaiu, M. Tanori, L. Di Magno, D. Bellavia, C. Capalbo, S. Puget, E. De Smaele, G. Canettieri, D. Guardavaccaro, L. Busino, A. Peschiaroli, S. Pazzaglia, G. Giannini, G. Melino, F. Locatelli, A. Gulino, O. Ayrault, D. Fruci, L. Di Marcotullio, ERAP1 promotes Hedgehog-dependent tumorigenesis by controlling USP47-mediated degradation of βTrCP, Nat. Commun. 10 (2019) 3304.
[27] R. Orlando, S. De Martin, L. Andrighetto, M. Floreani, P. Palatini, Fluvoxamine pharmacokinetics in healthy elderly subjects and elderly patients with chronic heart failure, Br. J. Clin. Pharmacol. 69 (2010) 279–286.
[28] B. Gidwani, A. Vyas, A comprehensive review on cyclodextrin-based carriers for delivery of chemotherapeutic cytotoxic anticancer drugs, BioMed Res. Int. 2015 (2015) 198268.
[29] Z. Sezgin, N. Yüksel, T. Baykara, Preparation and characterization of polymeric micelles for solubilization of poorly soluble anticancer drugs, Eur. J. Pharm. Biopharm. 64 (2006) 261–268.
[30] R.J. Braun, E.L. Parrott, Influence of viscosity and solubilization on dissolution rate, J. Pharmacol. Sci. 61 (1972) 175–178.
[31] J. Pitha, S.M. Harman, M.E. Michel, Hydrophilic cyclodextrin derivatives enable effective oral administration of steroidal hormones, J. Pharmacol. Sci. 75 (1986) 165–167.
[32] B. Karolewicz, M. Gajda, A. Gorniak, A. Owczarek, I. Mucha, Pluronic F127 as a suitable carrier for preparing the imatinib base solid dispersions and its potential in development of a modified release dosage forms, J. Therm. Anal. Calorim. (2017).
[33] E. Ambrosio, A. Podmore, A.L. Gomes Dos Santos, A. Magarkar, A. Bunker, P. Caliceti, F. Mastrotto, C.F. van der Walle, S. Salmaso, Control of peptide aggregation and fibrillation by physical PEGylation, Biomacromolecules 19 (2018) 3958–3969.
[34] T. Higuchi, A phase solubility technique, Adv. Anal. Chem. Instrum. 4 (1965) 117–211.
[35] C. Ingallina, P.M. Costa, F. Ghirga, R. Klippstein, J.T. Wang, S. Berardozzi, N. Hodgins, P. Infante, S.M. Pollard, B. Botta, K.T. Al-Jamal, Polymeric glabrescione B nanocapsules for passive targeting of Hedgehog-dependent tumor therapy in vitro, Nanomedicine 12 (2017) 711–728.
[36] S. De, A. Girigoswami, S. Das, Fluorescence probing of albumin-surfactant interaction, J. Colloid Interface Sci. 285 (2005) 562–573.
[37] Y. Moriyama, E. Watanabe, K. Kobayashi, H. Harano, E. Inui, K. Takeda, Secondary structural change of bovine serum albumin in thermal denaturation up to 130 degrees C and protective effect of sodium dodecyl sulfate on the change, J. Phys. Chem. B 112 (2008) 16585–16589.
[38] X. Li, Z. Yang, K. Yang, Y. Zhou, X. Chen, Y. Zhang, F. Wang, Y. Liu, L. Ren, Self-assembled polymeric micellar nanoparticles as nanocarriers for poorly soluble anticancer drug ethaselen, Nanoscale Res Lett 4 (2009) 1502–1511.
[39] P. Infante, R. Alfonsi, C. Ingallina, D. Quaglio, F. Ghirga, I. D'Acquarica, F. Bernardi, L. Di Magno, G. Canettieri, I. Screpanti, A. Gulino, B. Botta, M. Mori, L. Di Marcotullio, Inhibition of Hedgehog-dependent tumors and cancer stem cells by a newly identified naturally occurring chemotype, Cell Death Dis. 7 (2016), e2376.
[40] W. Li, M. Yalcin, D.J. Bharali, Q. Lin, K. Godugu, K. Fujioka, K.A. Keating, S. A. Mousa, Pharmacokinetics, biodistribution, and anti-angiogenesis efficacy of diamino propane tetraiodothyroacetic acid-conjugated biodegradable polymeric nanoparticle, Sci. Rep. 9 (2019) 9006.
[41] C. Gong, Y. Xie, Q. Wu, Y. Wang, S. Deng, D. Xiong, L. Liu, M. Xiang, Z. Qian, Y. Wei, Improving anti-tumor activity with polymeric micelles entrapping paclitaxel in pulmonary carcinoma, Nanoscale 4 (2012) 6004–6017.
[42] C.H. Wu, M.S. Coumar, C.Y. Chu, W.H. Lin, Y.R. Chen, C.T. Chen, H.Y. Shiao, S. Rafi, S.Y. Wang, H. Hsu, C.H. Chen, C.Y. Chang, T.Y. Chang, T.W. Lien, M. Y. Fang, K.C. Yeh, C.P. Chen, T.K. Yeh, S.H. Hsieh, J.T. Hsu, C.C. Liao, Y.S. Chao, H. P. Hsieh, Design and synthesis of tetrahydropyridothieno[2,3-d]pyrimidine scaffold based epidermal growth factor receptor (EGFR) kinase inhibitors: the role of side chain chirality and Michael acceptor group for maximal potency, J. Med. Chem. 53 (2010) 7316–7326.
[43] F.M.G. Cavalli, M. Remke, L. Rampasek, J. Peacock, D.J.H. Shih, B. Luu, L. Garzia, J. Torchia, C. Nor, A.S. Morrissy, S. Agnihotri, Y.Y. Thompson, C.M. Kuzan-Fischer, H. Farooq, K. Isaev, C. Daniels, B.K. Cho, S.K. Kim, K.C. Wang, J.Y. Lee, W. A. Grajkowska, M. Perek-Polnik, A. Vasiljevic, C. Faure-Conter, A. Jouvet, C. Giannini, A.A. Nageswara Rao, K.K.W. Li, H.K. Ng, C.G. Eberhart, I.F. Pollack, R. L. Hamilton, G.Y. Gillespie, J.M. Olson, S. Leary, W.A. Weiss, B. Lach, L. B. Chambless, R.C. Thompson, M.K. Cooper, R. Vibhakar, P. Hauser, M.C. van Veelen, J.M. Kros, P.J. French, Y.S. Ra, T. Kumabe, E. López-Aguilar, K. Zitterbart, J. Sterba, G. Finocchiaro, M. Massimino, E.G. Van Meir, S. Osuka, T. Shofuda, A. Klekner, M. Zollo, J.R. Leonard, J.B. Rubin, N. Jabado, S. Albrecht, J. Mora, T. E. Van Meter, S. Jung, A.S. Moore, A.R. Hallahan, J.A. Chan, D.P.C. Tirapelli, C. G. Carlotti, M. Fouladi, J. Pimentel, C.C. Faria, A.G. Saad, L. Massimi, L.M. Liau, H. Wheeler, H. Nakamura, S.K. Elbabaa, M. Perezpeña-Diazconti, F. Chico Ponce de León, S. Robinson, M. Zapotocky, A. Lassaletta, A. Huang, C.E. Hawkins, U. Tabori, E. Bouffet, U. Bartels, P.B. Dirks, J.T. Rutka, G.D. Bader, J. Reimand, A. Goldenberg, V. Ramaswamy, M.D. Taylor, Intertumoral heterogeneity within medulloblastoma subgroups, Canc. Cell 31 (2017) 737–754, e736.
[44] H. Kimura, J.M. Ng, T. Curran, Transient inhibition of the Hedgehog pathway in young mice causes permanent defects in bone structure, Canc. Cell 13 (2008) 249–260.
[45] E.M. Beauchamp, L. Ringer, G. Bulut, K.P. Sajwan, M.D. Hall, Y.C. Lee, D. Peaceman, M. Ozdemirli, O. Rodriguez, T.J. Macdonald, C. Albanese, J. A. Toretsky, A. Uren, Arsenic trioxide inhibits human cancer cell growth and tumor development in mice by blocking Hedgehog/GLI pathway, J. Clin. Invest. 121 (2011) 148–160.
[46] J. Kim, J.J. Lee, D. Gardner, P.A. Beachy, Arsenic antagonizes the Hedgehog pathway by preventing ciliary accumulation and reducing stability of the Gli2 transcriptional effector, Proc. Natl. Acad. Sci. U. S. A. 107 (2010) 13432–13437.
[47] W.Y. Au, S. Tam, B.M. Fong, Y.L. Kwong, Determinants of cerebrospinal fluid arsenic concentration in patients with acute promyelocytic leukemia on oral arsenic trioxide therapy, Blood 112 (2008) 3587–3590.
[48] E. Peer, S. Tesanovic, F. Aberger, Next-Generation Hedgehog/GLI Pathway Inhibitors for Cancer Therapy, Cancers (Basel), 2019, p. 11.
[49] K. Paál, J. Müller, L. Hegedûs, High affinity binding of paclitaxel to human serum albumin, Eur. J. Biochem. 268 (2001) 2187–2191.